

**The effect of reagent translational excitation on the dynamics of the reaction
 $\text{H}+\text{Cl}_2\rightarrow\text{HCl}(v',J')+\text{Cl}$**

P. A. Berg and J. J. Sloan

Citation: *The Journal of Chemical Physics* **100**, 1075 (1994); doi: 10.1063/1.466639

View online: <http://dx.doi.org/10.1063/1.466639>

View Table of Contents: <http://scitation.aip.org/content/aip/journal/jcp/100/2?ver=pdfcov>

Published by the [AIP Publishing](#)

Articles you may be interested in

[The effect of reagent translation on the reaction dynamics and the absolute reaction cross section of
 \$\text{H}+\text{H}_2\text{O}\rightarrow\text{OH}+\text{H}_2\$](#)

J. Chem. Phys. **100**, 1936 (1994); 10.1063/1.466546

[Effect of changing reagent energy on reaction dynamics. XI. Dependence of reaction rate on vibrational excitation in endothermic reactions \$\text{HX}\(v \text{ reag}\)+\text{Na}\rightarrow\text{H}+\text{NaX}\(X=\text{F},\text{Cl}\)\$](#)

J. Chem. Phys. **74**, 3400 (1981); 10.1063/1.441493

[Infrared chemiluminescence study of the effects of increased relative translation upon the reaction:
 \$\text{H}+\text{ICl}\rightarrow\text{HCl}\(v',J'\)+\text{I}\$](#)

J. Chem. Phys. **67**, 3401 (1977); 10.1063/1.435294

[Molecular beam reaction of K with HCl: Effect of translational excitation of reagents](#)

J. Chem. Phys. **60**, 3335 (1974); 10.1063/1.1681527

[Rates of the Endothermic Reactions \$\text{HCl}+\text{X}\(X=\text{I}, \text{Cl}\)\$ as a Function of Reagent Vibration, Rotation, and Translation](#)

J. Chem. Phys. **51**, 5716 (1969); 10.1063/1.1672004



The effect of reagent translational excitation on the dynamics of the reaction $\text{H} + \text{Cl}_2 \rightarrow \text{HCl}(v', J') + \text{Cl}$

P. A. Berg and J. J. Sloan

Department of Chemistry, University of Waterloo, Waterloo N2L 3G1, Canada

(Received 23 August 1993; accepted 1 October 1993)

We use fast time-resolved Fourier transform spectroscopy and low pressure infrared chemiluminescence techniques to determine the product energy distribution in the title reaction. We create the reagent hydrogen atoms with 2.3 eV of translational excitation by photofragmentation of H_2S at 193 nm, and observe the time evolution of the infrared chemiluminescence from the product $\text{HCl}(v', J')$ under single gas kinetic collision conditions. The initial vibrational distribution, determined from the first observation after creation of the H atoms is $P(v' = 1:2:3:4:5:6:7:8) = 1.0:0.84:0.74:0.59:0.34:0.24:0.17:0.13$. The initial HCl rotational distribution in each vibrational level is broad, showing no identifiable maximum. The fraction of the total available energy entering HCl vibration and rotation, respectively, are 0.19 and 0.10. The time evolution of the observed vibrational and rotational distributions gives information about the changes in the reaction dynamics consequent on reduction of the reagent translational energy.

INTRODUCTION

The hydrogen atom plus halogen molecule reactions, and the reaction $\text{H} + \text{Cl}_2 \rightarrow \text{HCl} + \text{Cl}$ in particular, have been used to establish many of the earliest and most important hypotheses of reaction dynamics. The dynamics of this reaction were established over 20 years ago, when reports of the angular distributions¹⁻³ and the internal excitation^{4,5} of its products first appeared. These results, which were confirmed in extensive later work,⁶⁻¹¹ showed that the HCl product is strongly backward scattered with respect to the initial H atom direction, and that it has moderate vibrational, but low rotational excitation. The angular distributions established that the reaction occurs via a preferred collinear configuration, which results in backscattering and implies a "rebound" mechanism. The internal energy distribution of the HCl indicates that the H atom approaches the Cl_2 closely before the Cl-Cl repulsion accelerates the halogen atoms apart. The resulting, predominantly "repulsive," release of the reaction exoergicity does not excite HCl rotation because the typical intermediate has a near-collinear configuration, and the center of mass of the HCl product is near the Cl nucleus. Neither does it create HCl vibration, because the H atom approaches the nearer Cl atom so rapidly that most of the repulsive energy release acts on the already-formed HCl rather than on the Cl atom alone. This imparts translational excitation to the diatomic molecule as a whole, and creates little vibrational excitation.

Early theoretical efforts interpreted these experimental results reasonably well. The success of early Franck-Condon treatments¹²⁻¹⁶ confirmed the "sudden" nature of the interaction. Semiempirical (DIM)¹⁷⁻¹⁹ and extended LEPS²⁰ calculations of the potential energy surface confirmed that the collinear configuration presented the minimum barrier to H atom approach and provided realistic activation energies for the reaction. Many other dynamics^{21,22} and model²³ calculations have been carried out on

this system, including exact collinear quantum,^{24,25} both collinear and three-dimensional quasiclassical trajectories,^{20,26-29} collinear quantum with information theoretic extrapolations,^{18,30,31} three-dimensional quantum,³² and reduced dimensionality quantum Franck-Condon³³⁻³⁵ treatments. These have succeeded in reproducing most of the important features of the internal energy distributions measured in the experiments. In many of the theoretical studies, the sudden nature of this reaction is used to make appropriate approximations which simplify the computations. This characteristic is important in the interpretation of the results to be presented later in this report.

Because of the success of the various treatments based on an assumed sudden behavior, it is clear that the H/Cl_2 reaction dynamics are simple. The reaction occurs in a single interaction of short duration, which occurs largely between the pair of atoms involved in the initial collision. Consequently, this reaction provides an excellent laboratory to test many aspects of reaction dynamics theory. This was recognized early in the study of this reaction, and substantial efforts were made to explore the effect of energy on its dynamics. The experimental techniques available at that time, however, were not capable of selecting specific reagent energies, so information of a qualitative nature was sought through variation of reagent temperatures instead. Thus, the effects of changing the reagent temperature on the dynamics of both the H/Cl_2 ^{27,36} and the analogous H/F_2 reaction³⁷ were explored in the early experiments. Heating the halogen molecule gave information on the combined effects of increased reagent vibrational and rotational excitation. The effect of increasing reagent translational excitation was examined by thermally dissociating H_2 in a high temperature source—a tungsten oven operated at temperatures near 3000 K. This produced H atoms with an average translational energy of ~ 30 – 40 kJ/mol.

These experiments provided qualitative information

about the effect of increased reagent excitation on the dynamics of the reactions. In particular, for the H/Cl_2 reaction, they showed that increasing the H atom translational temperature from 300 to 2650 K resulted in a small, but very distinct, shift downwards in the peak of the product HCl vibrational excitation. For 300 K reagents, the earliest measurement²⁷ found the HCl vibrational distribution to be $P(v' = 1:2:3:4) = 0.12:0.44:0.40:0.04$; later measurements¹¹ gave $P(v' = 1:2:3:4) = 0.14:0.40:0.40:0.05$, which agrees with the previous measurement to within the experimental errors. For reagents having a translational temperature of 2650 K, two measurements gave $P(v' = 1:2:3:4:5:6) = 0.26:0.31:0.30:0.08:0.04:0.01$ ²⁷ and $P(v' = 1:2:3:4:5:6) = 0.24:0.28:0.23:0.13:0.07:0.03$.³⁶ Although broader, these distributions have lower vibrational excitation than distributions created by the room temperature reactions. As a consequence of this downward shift, the average fraction of the available energy entering vibration³⁸ is reduced from ~ 0.39 for 300 K hydrogen atoms to ~ 0.30 for 2650 K hydrogen atoms. Simultaneously, there is a commensurate increase in the fraction of the energy appearing in rotation from ~ 0.08 to 0.12, and in translation from ~ 0.53 to 0.58.

These results have proven to be robust over the time since their enunciation, and many of our qualitative ideas about reaction dynamics are based on them. It is difficult, however, to extract quantitative information from these experiments. The very large spread of reagent energies and the uncertainties in the reagent energy distributions which are inherent in the thermal excitation technique make the precise definition of the reagent conditions problematic. Furthermore, the spread of reagent energies implies that the reagents sample a very large part of the potential energy surface simultaneously, so it is difficult to identify the specific details of the surface which are responsible for the observed effects. This, in turn, makes it difficult to carry out definitive calculations to interpret the experiments, because results which agree with the experiments qualitatively can be obtained from a variety of surfaces differing in those details which are averaged out by the large range of experimental energies. The calculations, therefore, cannot ensure that the correct surface has been uniquely identified.

We have carried out an experiment to examine the effect of translational excitation on the H/Cl_2 reaction using a specific, well-defined, and relatively high, reagent translational energy. This experiment permits the identification of the exact region of the potential energy surface sampled by the reaction, and hence permits the precise definition of the initial conditions appropriate for dynamics calculations to test this part of the surface.

We create the reagent hydrogen atoms using laser photofragmentation and observe the resulting internal energy distribution of the HCl product using low pressure infrared chemiluminescence techniques which are similar to those used in most of the earlier experimental work. The spectroscopic technique with which we make the observations, however, is time-resolved Fourier transform infrared spectroscopy, which permits the resolution of the product vibrational and rotational populations on a single collision

basis. This combination of precisely defined reagent energies and time-resolved product detection gives much more detailed information than the previous work, and provides results which can be used by theory to test specific regions of the potential energy surface.

EXPERIMENT

The fast time-resolved Fourier transform spectroscopy (FTRFTS) technique, which is essential to this experiment, has been described elsewhere.³⁹ The specific FTRFTS instrument used for this work is a revision of the instrument described in Ref. 39. It has been fully described as well,⁴⁰ and the details of the implementation will not be explained here. We shall, however, outline the essential aspects of the instrument, to provide a context for the results to be presented in later sections of this report.

The architecture is based on the VME bus, and uses a Motorola 68040 single board computer (SBC) as the basic engine. The system consists of the necessary hardware and firmware to control the experiment. The firmware is contained in PROMS mounted in the user-programmable sockets of the SBC, so the system is standalone. Under firmware control, the system provides a trigger for the excitation source which generates the transient, and collects and stores the time-resolved interferograms, which are Fourier transformed later. The firmware also provides a menu under which the user enters the desired timing for the excitation and data collection.

Our FTRFTS technique is designed to be used with a continuous-scan (as opposed to a step-scan) Michelson interferometer. It is compatible with any commercial continuous-scan interferometer, and the resulting spectral sensitivity and resolution depend on the interferometer only. The normal throughput and multiplex advantages of FTS are retained fully in time resolved operation. Our present FTRFTS instrument is capable of collecting up to 128 spectra with a time resolution (time between spectra) ranging from 1 ms to 1 μs . For the present experiment, we use a spectral resolution of 0.4 cm^{-1} . To obtain this, we collect about 40 000 data points on each time-resolved interferogram; these comprise about 1500 points before, and about 38 500 points after the zero path difference (ZPD) position. We phase correct the data in the customary way, using a short (2048 point) double-sided interferogram centered on the ZPD position. We Fourier transform the resulting interferogram by selecting 32 768 points after the ZPD and zero-filling by a factor of 2.

The translationally excited H atoms are created by photodissociation of H_2S using a 193 nm excimer laser (Lumonics Excimer 6000). This laser is a slightly modified version of the conventional Excimer 6000, designed by Lumonics for high repetition rate operation. It produces $\sim 25\text{--}30 \text{ W}$ of 193 nm (ArF) power at a repetition rate of 400 Hz.

The vacuum system and optical configuration were designed for conventional low-pressure infrared chemiluminescence experiments. The cylindrical stainless steel reaction chamber is evacuated through a 12 in. slide valve and 16 in. cryobaffle by a 15 in. diffusion pump (Varian VHS

400), backed by a Roots pump (Edwards EH-500) and mechanical pump (Edwards E2M-80). The cryobaffle is held at -30°C to minimize backstreaming.

The reagents, Cl_2 and H_2S , are admitted into the reaction volume via concentric quartz inlet tubes mounted on the top center axis of the reaction chamber. This inlet is designed to mix the reagents immediately before they are admitted into the region irradiated by the laser. The ArF excimer laser beam is positioned just below the inlet, to intersect as much of the entering reagent mixture as possible. For the present experiments, the reagents were admitted to the main chamber in equal quantities, each having a partial pressure of $\sim 1.5 \times 10^{-2}$ Torr.

At the total pressure of this experiment (3×10^{-2} Torr), the mean free path is $\sim 1.7 \times 10^{-3}$ m and, depending on the masses of the molecules involved, the average gas kinetic collision time is $\sim 3 \times 10^{-6}$ s. The H atoms created in the photodissociation have a very high velocity ($\sim 2 \times 10^4$ m/s), and they suffer their first collision, on the average, $\sim 8 \times 10^{-8}$ s after the ArF laser pulse. (The laser pulse has a temporal length of $\sim 1 \times 10^{-8}$ s, which is shorter than any of the other characteristic times of the experiment.) Following a reactive collision, the HCl product can have a range of translational velocities from near zero, to 4.7×10^3 m/s, which is the limit imposed by the total energy available to the products (410.9 kJ). For the HCl molecules with the highest velocities (those created in the lowest vibrational level with no rotational energy), the first collision, on the average, occurs at 3.6×10^{-7} s after the reaction. The maximum available product translational energy decreases with increasing vibrational excitation, and for $\text{HCl}(v'=2)$ the first collision would occur at 4.0×10^{-7} s; for $\text{HCl}(v'=4)$, 4.4×10^{-7} s; for $\text{HCl}(v'=8)$, 5.5×10^{-7} s, etc. We assume that the excess translational energy of the HCl product is lost at approximately the first collision, so that subsequent collisions occur, on the average, at the gas kinetic collision time appropriate to the 300 K background gas in the chamber. For HCl colliding with an "average" collider having a mass equal to the average of Cl_2 and H_2S , the gas kinetic collision time is 3.1×10^{-6} s.

The first collision between a H atom and a Cl_2 molecule is not always reactive, of course, and as a result of the nonreactive inelastic collisions, H atoms with reduced translational energies begin to accumulate at longer times. These react with the remaining Cl_2 and produce vibrationally excited HCl, which is observed at later time delays. The vibrational distribution of the HCl produced in these later reactions involving reagents with lower translational energies should be, in the limit of complete thermalization of the H atoms, the same as that observed in the early experiments using 300 K thermal reagents.

We designed the timing for the data collection in the present experiments to examine only the first few collisions after the creation of the hydrogen atoms. We programmed the FTRFTS data acquisition system to record a total of 16 time-resolved spectra, with a separation between successive observations of $1.5 \mu\text{s}$, for a total observation time of $22.5 \mu\text{s}$. We specified that two spectra be recorded before triggering the excimer laser, to establish background emission

levels. The FTRFTS hardware triggered the laser ~ 100 ns before recording the third spectrum.

Following the laser pulse, a transient with a rise time of $2 \mu\text{s}$ (0%–90%) appears on the output of the infrared detector's amplifier. The electrical bandwidth of the detector–amplifier chain is 1 MHz, so the rise time of the transient is not detector limited; it reflects the rate of the gas phase reaction. After triggering the laser, the FTRFTS data acquisition system recorded 14 more spectra at intervals of $1.5 \mu\text{s}$, for a total time of $19.5 \mu\text{s}$ after the laser was fired.

The remaining information about the experiment is the same as that for conventional laser photodissociation/infrared chemiluminescence work. The light path of the excimer laser is flushed with dry nitrogen to prevent the formation of ozone, and the infrared collection optics are surrounded by a dry-ice-cooled shroud to reduce the background emission in the observation region and scavenge any products of reactions involving sulfur compounds formed in the photofragmentation. The H_2S and Cl_2 were obtained from Linde Division of Union Carbide Canada Ltd. and Standchem Co. Ltd. and used without purification.

RESULTS

A sample of the spectra obtained in this experiment are shown in Fig. 1. Time increases from the lower to the higher panels. As described in the Experiment, we recorded two spectra before triggering the laser, then 14 after. In the following discussion, we shall take the zero of time to be the point at which the laser fires, 100 ns before the third spectrum which we recorded. All spectra were separated by a time delay of $1.5 \mu\text{s}$, so the total observation time after firing the laser is $19.5 \mu\text{s}$. The lowest spectrum in Fig. 1(a), labeled $-1.5 \mu\text{s}$, is the one recorded just before the laser was triggered. We do not show the spectrum recorded just before this one (at $-3.0 \mu\text{s}$); it is identical to the one at $-1.5 \mu\text{s}$. As expected, the spectra at -3.0 and $-1.5 \mu\text{s}$ contain no HCl signal, only the background emission.

The first spectrum in Fig. 1(a), recorded at $-1.5 \mu\text{s}$, shows only the base line. This shape is determined by the 300 K blackbody emission from the surroundings, modified by the detectivity of the InSb detector, which has its low-energy cutoff at $\sim 1850 \text{ cm}^{-1}$. The light path in the interferometer is not purged, so the background shows absorption features from atmospheric water (the sharp features between 1850 and 2000 cm^{-1}) and from CO_2 (the broad feature at $\sim 2350 \text{ cm}^{-1}$).

The second spectrum in Fig. 1(a), labeled $0 \mu\text{s}$, was recorded ~ 100 ns after triggering the laser. Most of the fast H atoms collide with Cl_2 during the time interval between the laser pulse and the recording of the second spectrum (*vide supra*). No signal is evident in the spectrum at $0 \mu\text{s}$, however, because the rise time of the detector/amplifier electronics ($\sim 1 \mu\text{s}$) is too slow to respond to the emission from the HCl product on this time scale. Close inspection of this spectrum shows traces of emission from

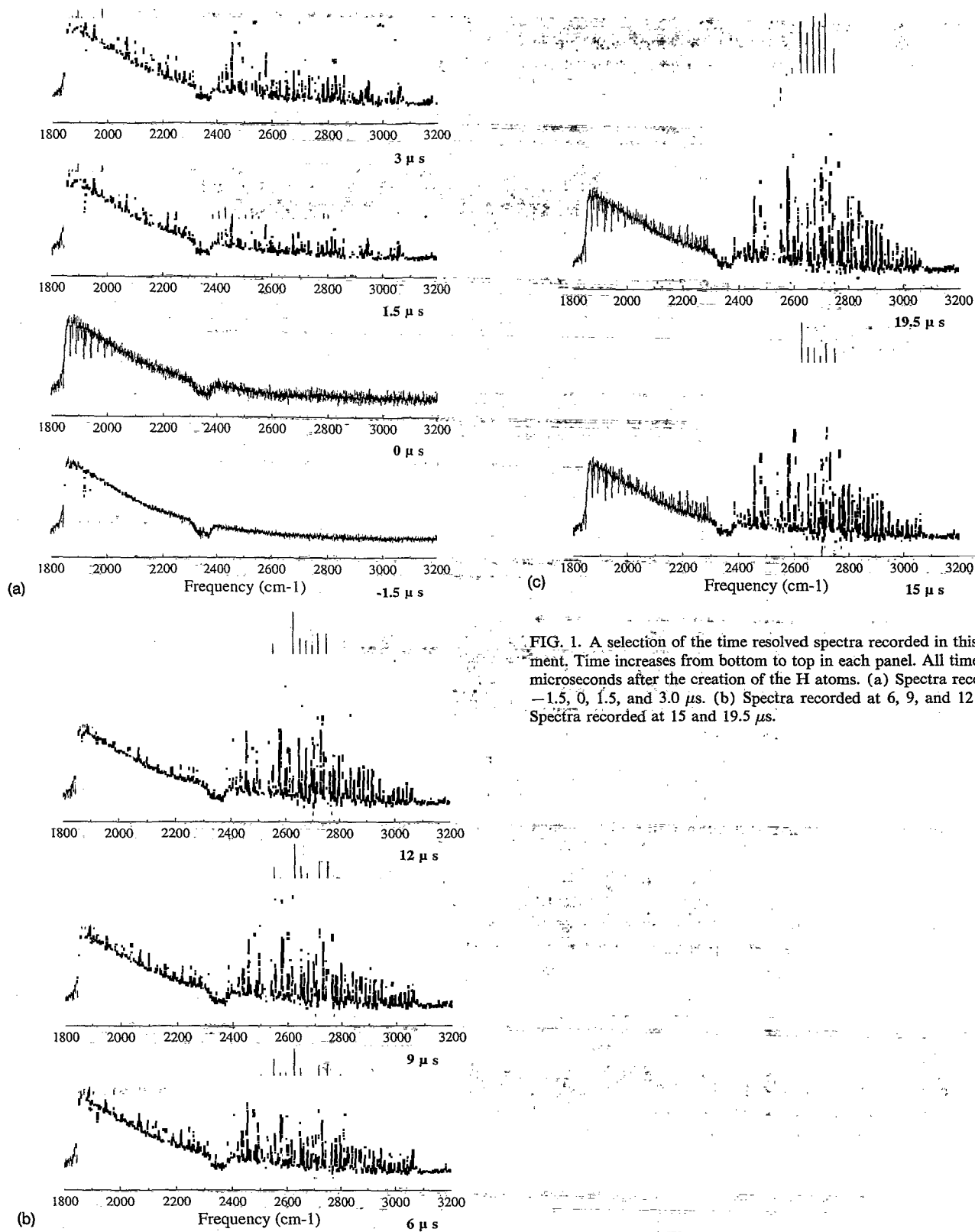


FIG. 1. A selection of the time resolved spectra recorded in this experiment. Time increases from bottom to top in each panel. All times are in microseconds after the creation of the H atoms. (a) Spectra recorded at -1.5 , 0 , 1.5 , and $3.0 \mu\text{s}$. (b) Spectra recorded at 6 , 9 , and $12 \mu\text{s}$. (c) Spectra recorded at 15 and $19.5 \mu\text{s}$.

HCl, but the signal to noise ratio is very low, and we do not derive any quantitative information from it.

Strong, identifiable HCl emission, with a signal to noise ratio greater than ten, is evident in the third spectrum in Fig. 1(a), taken at $1.5 \mu\text{s}$ after firing the laser. We have pointed out previously that the first reactive collision involving the translationally excited H atoms occurs ~ 80 ns

after the laser pulse, and the first collision of the HCl product occurs ~ 300 – 500 ns after the reaction. Since the rise time of the electronics is $\sim 1 \mu\text{s}$, the emission recorded in this spectrum should not be electronically distorted. We note parenthetically that even if there is electronic distortion at this time, the *relative* intensities of the spectral transitions will not be affected—only their *absolute* values. We

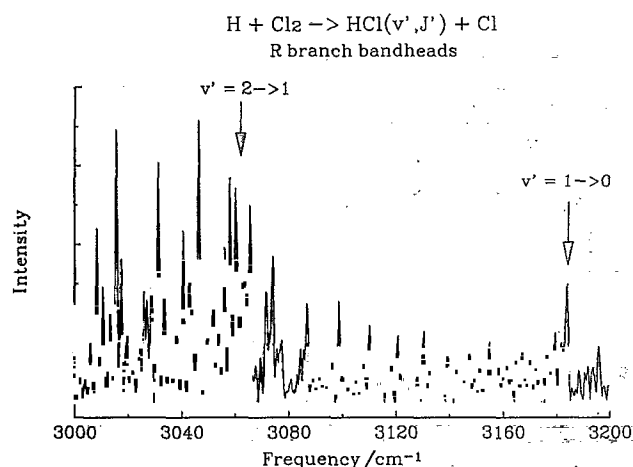


FIG. 2. The spectral region of the HCl fundamental *R* branch bandheads of $v' = 1 \rightarrow 0$ and $2 \rightarrow 1$ transitions, showing the buildup of intensity at the bandheads due to the very high HCl rotational states created in the reaction. In the $v' = 1$ emission, rotational states up to $J' = 35$ could be identified.

assume that the HCl is translationally thermalized in approximately the first collision. The gas kinetic collision time for HCl molecules having a 300 K thermal energy distribution in our experiment is $\sim 3 \mu\text{s}$. In view of this timing sequence, therefore, we conclude that the HCl recorded at $1.5 \mu\text{s}$ has had at most one collision since being created in the reaction, and we identify the energy distributions based on this spectrum as representing the HCl newly-created in the reaction—before collisional energy transfer has occurred.

The very large number of transitions in the spectrum recorded at $1.5 \mu\text{s}$ demonstrates that many vibrational and rotational states are created in the reaction. In this spectrum, we have identified HCl emission from vibrational levels up to $v' = 8$. For the lower vibrational levels, we can identify emission from rotational levels up to $J' = 35$. Most of the intense lines at low energy in this spectrum are *P* branch lines with very high rotational quantum numbers. The extremely high rotational excitation is illustrated in Fig. 2, which is the region of the *R*-branch bandheads of the $1 \rightarrow 0$ and $2 \rightarrow 1$ transitions. The locations of the two bandheads are indicated by vertical arrows, and the buildup of intensity due to the bandheads is quite evident. In both cases, the transition at the bandhead is $R(26)$, and for HCl($v' = 1$), the highest rotational quantum number identified unambiguously is $J' = 35$.

Figures 1(b) and 1(c) show a selection of the spectra recorded at later times. In each case, the time at which the spectrum was recorded is shown below the base line. The dramatic increase in the low (v', J') populations is clearly evident in the region between 2300 and 3100 cm^{-1} . Most of this increase is in the low rotational states of the first four vibrational levels. On average, only eight collisions involving the HCl reaction product occur during the entire observation period, and consequently, we expect virtually no vibrational deactivation and only a very small amount of rotational deactivation during this time. We shall show

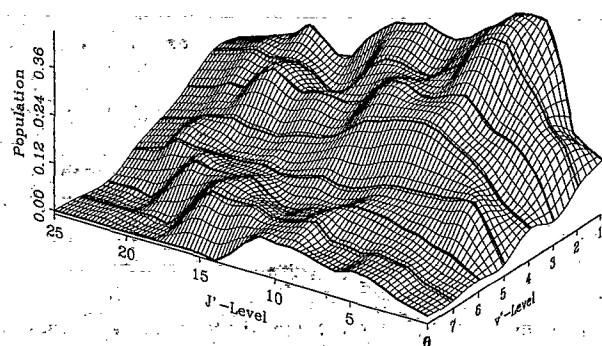


FIG. 3. The initial rotational distributions for all vibrational levels observed in the experiment. The rotational populations for individual vibrational levels are connected by heavy black lines. A three-dimensional spline is used to interpolate among the observed populations to illustrate how the reaction populates the HCl(v', J') space.

later in this section that the increase in HCl($v' \leq 4$) intensity is not due to vibrational deactivation, but to the reaction between Cl_2 and H atoms which have lost some of their translational energy in previous nonreactive collisions.

All lines in all of the spectra shown in Fig. 1 can be assigned to the fundamental emission bands of vibrationally excited HCl. About 25% of the HS from the photodissociation of H_2S at 193 nm is created in vibrationally excited levels,⁴¹ and we observe first overtone emission from this vibrationally excited HS in the spectral region between 4800 and 5800 cm^{-1} . The $v = 1 \rightarrow 0$ fundamental band origin is at 2599 cm^{-1} , and it might be expected that the HS fundamental would interfere with the measurement of the HCl intensities. The transition probabilities of the HS fundamental are lower than those of the overtone, however, and we are unable to discern any HS fundamental emission in the spectra shown in Fig. 1. Thus HS(v) provided no interference with the HCl spectral analysis.

We processed the spectra using data analysis software written in this laboratory. This package of programs uses a library of highly accurate HCl transition frequencies to assign the spectra, then deconvolutes all partly overlapping transitions with a routine based on a Gaussian fit to the instrumental line shape. This procedure determines the intensity of each transition and calculates the populations of the HCl(v', J') states using the known Einstein *A*-factors.⁴²

In the following few paragraphs, we shall present the HCl(v', J') populations which we derive from the intensities in the third spectrum in Fig. 1(a) (time = $1.5 \mu\text{s}$). As indicated previously, we believe this gives the initial HCl energy distributions from the reaction. The global population distribution is plotted in Fig. 3 as a surface in HCl(v', J') space. The height of the surface indicates the population at the indicated vibrational-rotational state. Reference to Fig. 1(a) shows that the spectrum from which this result is derived has the smallest intensity of any spectrum in the dataset. The noise level, on the other hand, is the same for all spectra in the dataset. As a consequence, the distribution shown in Fig. 3 has the lowest signal to noise ratio of all of the distributions reported in this paper.

The small-scale structure in the surface is noise, and hence this is the absolute noise level in the other distributions as well.

Figure 3 shows that the rotational states within each vibrational level are populated about equally, and there is virtually no correlation between the vibrational and rotational energy distributions. The reaction populates a broad range of vibrational and rotational levels, with a marked preference for low vibrational levels (*vide infra*) and a very slight preference for low rotational levels. Within the signal to noise level of our experiment, therefore, we conclude that for each vibrational level created, the reaction populates a broad distribution of rotational states with approximately equal probability. From these initial rotational distributions, we calculate that the fraction of the total energy released into HCl rotational excitation³⁸ is 0.10 ± 0.02 .

The initial product rotational distributions obtained in the present work are quite different from those recorded in the lower energy thermal experiments. For reagents with a 300 K thermal energy distribution, the HCl product rotational distribution has a single maximum, which peaks between $J' = 9$ and 12, and has a weak inverse dependence on vibrational state—higher rotational excitation occurs in the lower HCl vibrational levels.^{4,5,11} The experiments with a temperature of 2650 K^{27,36} give somewhat more-excited HCl rotational distributions, which have two maxima in each vibrational level, rather than one. One maximum occurs at approximately the same location as observed in the 300 K experiments, and another appears at much higher rotational levels, around $J' = 20$ –24.

For each rotational state, the population at the lower vibrational levels is greater than that at the higher ones. When all the rotational levels within a single vibrational level are summed, the result indicates a strong propensity for creation of the lower vibrational levels. As a consequence, the initial vibrational distribution implied by Fig. 3 is quite different from that observed for reaction at lower reagent translational energy. The vibrational distribution determined from the spectrum recorded at 1.5 μS [Fig. 1(a)] is $P(v' = 1:2:3:4:5:6:7:8) = 1.0:0.84:0.74:0.59:0.34:0.24:0.17:0.13$. This result indicates that the fraction of the total available energy released into HCl vibration³⁸ by the reaction involving 2.3 eV hydrogen atoms, is only 0.19. In making this calculation, we included an estimated population of $\text{HCl}(v' = 0)$, which we obtained by extrapolating the measured vibrational distribution. The complete vibrational distribution obtained in this way is $P(v' = 0:1:2:3:4:5:6:7:8) = 0.23:0.19:0.16:0.14:0.11:0.07:0.05:0.03:0.02$. (We did not extrapolate the surprisal plot for this purpose, because in this case, as in other examples of this mass combination,¹¹ the surprisal is strongly nonlinear.)

For comparison with the above results, the measurements^{4,5,11} using reagents having a 300 K thermal translational energy distribution (average collision energy $\langle T \rangle = 0.025$ eV), yield a strongly inverted HCl vibrational distribution, $P(v' = 1:2:3:4:5) = 0.14:0.40:0.40:0.05:0.01$. The measurements^{27,36} in which the H atoms have a 2650 K thermal translational energy distribution (average collision energy, $\langle T \rangle = 0.45$ eV) reported less-inverted HCl vibrational distributions, $P(v' = 1:2:3:4:5:6) = 0.83:1.00:0.86:0.26:0.13:0.04$,²⁷ and $P(v' = 1:2:3:4:5:6) = 0.89:1.00:0.84:0.47:0.26:0.11$.³⁶

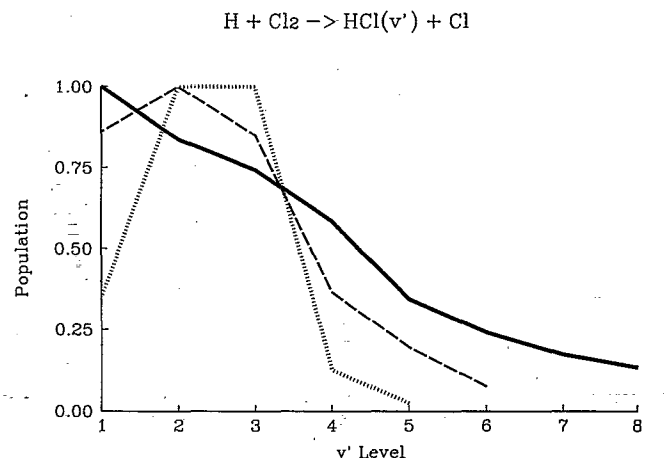


FIG. 4. The initial vibrational distribution created by the $\text{H} + \text{Cl}_2$ reaction is given by the solid curve. The dashed curve gives the vibrational distribution from 2650 K thermal hydrogen atoms (Refs. 27 and 36). The dotted curve is the result if room temperature thermal hydrogen atoms are used (Refs. 4, 5, and 11).

Figure 4 compares the HCl vibrational distributions obtained for the two different thermal reagent energy distributions with that obtained in the present work, at a single reagent translational energy, $T = 2.3$ eV. Our measurement is given by the solid line; it shows that the populations decrease monotonically with increasing vibrational quantum number. The average of the two measurements done using reagents having a translational temperature of 2650 K is shown by the dashed curve. The corresponding result for reagents having a translational temperature of 300 K is given by the dots. This comparison shows that increasing the reagent translational energy dramatically shifts the product HCl vibrational distribution to lower levels.

The behavior of the HCl product energy distributions with time, which we obtain in our time resolved measurements, also gives information about the dependence of the dynamics on collision energy. The progression of vibrational distributions obtained from the spectra recorded at later times are shown as the solid lines in Fig. 5. The distribution obtained in the 2650 K thermal experiments is shown as a dashed line in the figure, and that from the 300 K thermal experiments is given by the dotted line. The solid lines show the distributions from alternate spectra recorded in our experiment, starting from 1.5 μS (the lowest curve) then 4.5 μS , 7.5 μS , etc., up to 19.5 μS (the highest curve). Clearly, the populations of the lower vibrational levels increase rapidly with time, whereas those of the higher levels do not change much. The rapid increase in the populations of the lower levels cannot be due to collisional deactivation from the upper levels, for two reasons. First, only one gas kinetic collision occurs between

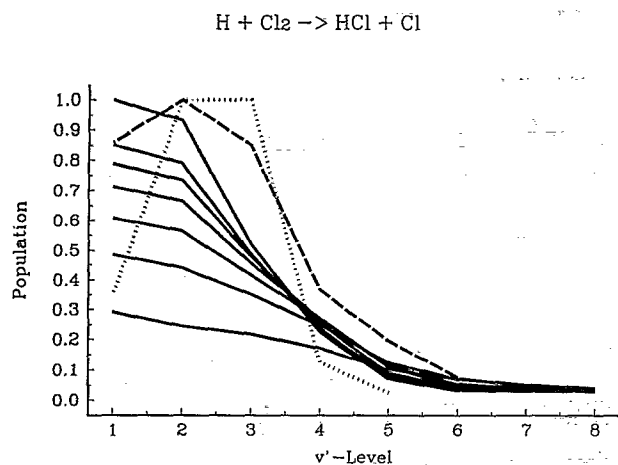


FIG. 5. The time evolution of the measured vibrational distributions is given by the solid curves. The solid curves (from lowest to highest) show the vibrational distributions measured at 3 μs intervals from 1.5 to 19.5 μs after the creation of the hydrogen atoms. The dashed and dotted curves are as in Fig. 4.

each distribution, and the deactivation rate cannot be that fast. Furthermore, there is no evidence, on this time scale, for disappearance of enough population from the higher vibrational populations to account for the increase in population in the lower levels. Hence, we conclude that the increase in populations of the levels $v' \leq 4$ must be due to a reaction which continues to occur during the few collisions over which these observations are made.

Comparison of these distributions with the one obtained in the 2650 K thermal experiments (the dashed line in Fig. 5) suggests that the populations recorded in our experiment appear to be evolving towards the latter. In particular, for the later time delays, the reaction rate into the higher vibrational levels ($v' > 4$) is virtually zero, while that into the lower levels ($v' < 4$) is substantial. This may be evidence for the fact that the distributions measured at later times in our experiment are created in reactions involving H atoms which have lost some of their translational energy in previous, nonreactive, collisions. That the H atoms do not become thermalized on the first collision can be ascribed to the large mass difference between the H atoms and the most probable collision partners, Cl_2 and H_2S . Furthermore, as indicated earlier, we expect that the reactive cross section increases with decreasing translational energy, so the rate of production of HCl in these lower-energy collisions may actually increase with time despite the reduction in the H atom concentration.

If this hypothesis is correct, then the later rotational distributions should show evidence for the bimodal rotational distribution reported in the 2650 K thermal experiments. In Fig. 6, we show the initial rotational distributions corresponding to the vibrational distributions given in Fig. 5. Only the rotational distributions for vibrational levels one through four are shown; the vibrational quantum number increases from bottom to top. Our measured time-dependent distributions are shown by the

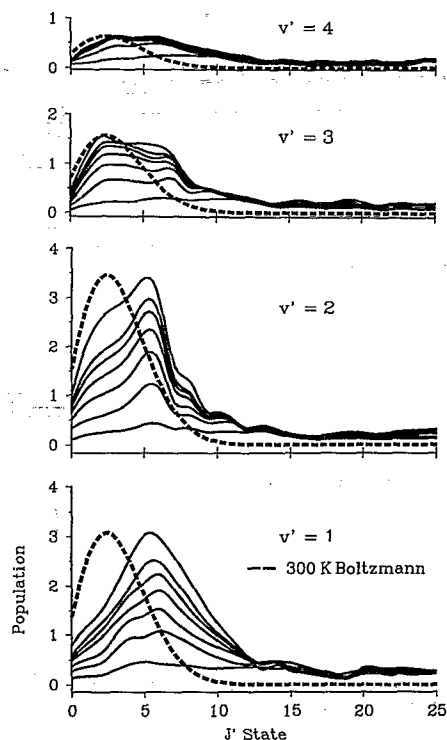


FIG. 6. The time evolution of the rotational distributions for the first four vibrational levels. The order of the curves in each panel (lowest to highest) corresponds to the order of the vibrational distribution curves given by the solid lines in Fig. 5. The dashed curves are 300 K Boltzmann HCl rotational distributions for comparison.

solid curves; the time delays correspond to those in Fig. 5—the lowest curve in each case corresponds to the signal at 1.5 μs after the laser is triggered, and the remaining ones are alternate measurements up to the highest curve, which is for 19.5 μs after the laser fires. The dashed curves in each panel give 300 K Boltzmann rotational distributions for HCl in each of the v' levels. We note that the detailed distribution shown in Fig. 3 corresponds to the lowest curve in Fig. 6, and that the absolute size of the noise indicated by the small scale structure in Fig. 3 is the same for all subsequent distributions. Since the signal grows rapidly with time, the signal to noise ratio increases with time.

The results in Fig. 6 show that the initial rotational distributions show no preference for population of a particular group of rotational states. Unlike the distributions reported for the 2650 K thermal experiments, there is no distinguishable excess population in the rotational states around $J' = 20$ in any of the late-time distributions. Furthermore, the maximum at low energy, around $J' = 10$, reported in both the 2650 K experiments and the 300 K experiments, is absent as well. In place of these maxima, the predominant feature of the later rotational distributions is a large maximum which occurs at about $J' = 6$ in each vibrational level. This maximum becomes larger with time. Furthermore, it is increasingly asymmetrical with increasing vibrational quantum number. A shoulder at low rotational energy is just discernible for $v' = 2$, and becomes

increasingly prominent (relative to the height of the maximum at $J' = 6$) for the third and fourth vibrational states.

The prominent maximum at $J' = 6$ in each vibrational state is not caused by rotationally relaxed HCl. The maximum of the Boltzmann rotational distribution for HCl at 300 K occurs between $J' = 2$ and 3, as indicated by the dashed curves in each panel of Fig. 6. Clearly, the 300 K Boltzmann distributions coincide with the low- J' shoulders on the larger ($J' = 6$) maxima, and we ascribe these shoulders to rotationally relaxed HCl. The shoulders are less obvious in the lower vibrational levels, especially in $v' = 1$; they become increasingly prominent with respect to the $J' = 6$ maxima in the higher vibrational levels. The relative heights of the two maxima, of course, are determined by the relative rates of the processes populating them. The rate constant for rotational relaxation is approximately the same for all vibrational levels, so it is clear that the reaction which populates the $J' = 6$ peak has a higher rate constant for the lower vibrational levels than for the higher ones. This resembles our result for the initial vibrational distribution at a hydrogen translational energy of 2.3 eV, and indicates that the translational energy of the hydrogen involved in these later reactions is still high.

We conclude that the shoulder at $J' = 3$ in the later-time observations is caused by rotationally relaxed HCl. The maxima at $J' = 6$ in these later observations probably have the same dynamical origin as those observed at low J' in the lower-energy thermal experiments. The locations of the low- J' maxima in both the 300 and 2650 K thermal experiments have virtually no vibrational dependence, just as is observed in our result. These maxima were ascribed to reaction at predominantly collinear geometries in the thermal experiments, and this may be the case in our later-time results as well. In both cases, however, the maxima from the lower energy reactions occur at higher J' values than observed in our results. It is not clear why this should occur. The rationalization for this observation will require dynamical calculations on potential energy surfaces which accurately reproduce the behavior of the system at the higher energies sampled in our experiments.

The fact that the rotational distributions recorded in our later spectra differ from those of the 2650 K experiments suggests that the reagent energies in our later observations are still considerably higher than the 0.45 eV average energy of the 2650 K experiments. This is borne out by the vibrational distributions shown in Fig. 5. Although the trend is evident, even the final distribution recorded in our experiment has considerably less vibrational excitation than that of the 2650 K experiment, which is clearly inverted in the $v' = 2/v' = 1$ ratio. Furthermore, there is a small amount of rotational deactivation in our later-time results, and this would compete against any reaction which populates the higher J' states.

DISCUSSION AND CONCLUSIONS

We find that the reaction of H atoms with Cl_2 at extremely high relative translational energy yields HCl having very low vibrational, and only moderate rotational excitation. The reaction involving hydrogen atoms with 2.3

eV of translational energy, releases only 19% of the total available energy into HCl vibration. This result may be compared with corresponding values of 29% to 33% for reaction with hydrogen atoms at 2650 K^{27,36} ($\langle T \rangle = 0.45$ eV), and 39% for hydrogen atoms at 300 K^{4,5,11} ($\langle T \rangle = 0.025$ eV). For hydrogen atoms at 2.3 eV, the HCl vibrational distribution decreases monotonically with increasing vibrational level, $P(v' = 0:1:2:3:4:5:6:7:8) = 0.23:0.19:0.16:0.14:0.11:0.07:0.05:0.03:0.02$. The vibrational distributions created by reaction at lower kinetic energy are inverted.

The fraction of the total energy released into HCl rotational excitation, derived from our initial distributions, is 0.10 ± 0.02 . This is not significantly different from the result obtained at 2650 K (0.11 ± 0.02), or the 300 K result (0.08 ± 0.01). It thus appears that there is an upper limit on the rotational excitation which this reaction creates. The initial rotational distributions determined in the present work do not resemble the results of either of the thermal experiments. Our measurements indicate that at a reagent energy of 2.3 eV, no specific subset of product rotational states is populated preferentially. This can be seen from the very broad rotational distributions in each vibrational level shown in Fig. 3. The simplest interpretation of this result is that the reagent translational energy of our experiment is very much higher than the barrier to approach at any angle, so the reaction intermediate is not limited to collinear, or any other specific, geometry.

At longer observation times in our experiment, we see the products of reaction involving hydrogen atoms which have lost some of their translational energy. In these reactions, the HCl product rotational distribution has a maximum at about $J' = 6$ in all vibrational levels. The reaction at 300 K has a single maximum at slightly higher rotational energy (about $J' = 9-12$), while the reaction at 2650 K has two maxima—one at the same location as the 300 K distributions, and a second at $J' = 20-24$.

The origin of the single maximum at low product rotational states in the 300 K experiments is attributed to the fact that the minimum energy path on the potential energy surface occurs for collinear geometry. The barriers to approach in bent geometries are too high to permit reaction at low translational energy, so the dynamics are predominantly collinear and direct. The center of mass of the departing HCl is very near the Cl nucleus, so the repulsion released during product separation primarily acts on the Cl end of the HCl, and along the Cl-H bond. This mechanism does not generate much HCl rotation. (Differential cross section measurements confirm this model; the HCl product is found to be strongly backward scattered in the center of mass frame.^{1,2})

The reports of the 2650 K experiments speculate on two possibilities for the bimodal rotational distribution observed in that case. The maximum at lower rotational energy is thought to arise from the same dynamics as that in the 300 K reaction, while the higher-energy maximum is ascribed to either the opening of a second reaction channel at noncollinear geometry, or the existence of "microscopic

branching" in which the final reaction occurs at a site other than the one at which the initial encounter took place.⁴³

Any model of the high energy reaction must take into account the fact that the reactive cross section is a strong function of the relative translational energy. The $\text{H} + \text{Cl}_2$ reaction has an "early barrier," and thus the cross section increases with translational energy at low energies near the barrier. Eventually, however, the cross section must decrease with increasing translational energy, and this process may have begun at 2.3 eV. If this is so, then the initial orbital angular momentum may not be very large, despite the large value of the relative velocity, since both the reduced mass and the impact parameter may be small. There is a substantial contribution to the reagent angular momentum from Cl_2 rotation, however, which peaks at about $J=20$.

The product angular momentum disposal for a direct reaction on a predominantly repulsive potential energy surface is a function of the reactive impact parameter and the preferred geometry of the collision. In the present case, the energy barriers to approach are unlikely to be higher than the reagent translational energy for any approach geometry, so we expect that all reactive geometries are possible. In going from reagents to products, the reduced mass increases by a factor of 18, and the average relative translational energy of the products is high. By energy conservation, the average product translational excitation is 71% of the total available energy, or 292 kJ/mol. Using this energy, we calculate that for equal values of the reagent and product impact parameters, the average product orbital angular momentum is a factor of 5 larger than the reagent orbital angular momentum.

The observed initial rotational distribution is very broad, having population up to $J'=25$ in most low vibrational levels. This only represents ~ 80 kJ/mol of rotational energy, however, which is much less than E'_{tot} (410.9 kJ/mol), so there is no energy constraint on the observed rotational distributions. Reaction at bent geometries with repulsive energy release causes high product rotational excitation, although this effect is somewhat reduced in the present case because the repulsion is released on the center of mass of the Cl atom, which does not generate HCl rotation efficiently. The appearance of high rotational states, however, indicates that the reaction at high relative translational energy is not constrained to occur via linear geometry. The absence of a second maximum in the product rotational distribution is a notable difference from the results observed at intermediate translational energy. We cannot speculate on the cause of this difference based on the information which we have available at present.

Dynamical calculations will be required to elucidate the causes of the results we observe in this reaction. We believe that if such dynamical calculations are carried out, they will place extremely stringent limits on the potential energy surface, especially on those parts of it which describe the reagent approach coordinate. The initial conditions of our experiment are sufficiently well-defined that all ambiguity in specifying the initial conditions for such a calculation is removed. Furthermore, a global potential en-

ergy surface of high accuracy will be required in order to reproduce both the results of our experiments and those of the lower energy studies.

ACKNOWLEDGMENTS

We acknowledge support for this work from the Natural Sciences and Engineering Research Council of Canada, and from the Center of Excellence for Molecular and Interfacial Dynamics.

- ¹D. R. Herschbach, *Faraday Discuss. Chem. Soc.* **55**, 233 (1973).
- ²J. D. McDonald, P. R. LeBreton, Y. T. Lee, and D. R. Herschbach, *J. Chem. Phys.* **56**, 769 (1972).
- ³J. Grosser and H. Haberland, *Chem. Phys.* **7**, 442 (1970).
- ⁴K. G. Anlauf, P. J. Kuntz, D. H. Maylotte, P. D. Pacey, and J. C. Polanyi, *Faraday Discuss. Chem. Soc.* **44**, 183 (1967).
- ⁵K. G. Anlauf, D. S. Horne, R. G. Macdonald, J. C. Polanyi, and K. B. Woodall, *J. Chem. Phys.* **57**, 1561 (1972).
- ⁶J. P. Sung and D. W. Setser, *Chem. Phys. Lett.* **58**, 98 (1978).
- ⁷K. Tamagake and D. W. Setser, *J. Phys. Chem.* **83**, 1000 (1979).
- ⁸J. P. Sung, R. J. Malins, and D. W. Setser, *J. Phys. Chem.* **83**, 1007 (1979).
- ⁹W. Bardorff and H. Heydtmann, *Ber. Bunsenges. Phys. Chem.* **82**, 649 (1978).
- ¹⁰B. E. Holmes and D. W. Setser, in *Physical Chemistry of Fast Reactions*, edited by I. W. M. Smith (Plenum, New York, 1980), Vol. 2, Chap. 2.
- ¹¹M. A. Wickramaaratchi, D. W. Setser, B. Hildebrandt, B. Korbitzer, and H. Heydtmann, *Chem. Phys.* **84**, 105 (1984).
- ¹²G. C. Schatz and J. Ross, *J. Chem. Phys.* **66**, 10 (1977).
- ¹³G. C. Schatz and J. Ross, *J. Chem. Phys.* **66**, 1037 (1977).
- ¹⁴G. C. Schatz and J. Ross, *J. Chem. Phys.* **66**, 2943 (1977).
- ¹⁵C. L. Vila, J. L. Kinsey, J. Ross, and G. C. Schatz, *J. Chem. Phys.* **70**, 2414 (1979).
- ¹⁶C. L. Vila, D. J. Zvijac, and J. Ross, *J. Chem. Phys.* **66**, 62 (1977).
- ¹⁷I. Last, *Chem. Phys.* **69**, 193 (1982).
- ¹⁸I. Last and M. Baer, *J. Chem. Phys.* **80**, 3246 (1984).
- ¹⁹J. J. Duggan and R. Grice, *J. Chem. Soc. Faraday Trans. 2*, 729 (1984).
- ²⁰J. N. L. Connor, W. Jakubetz, J. Manz, and J. C. Whitehead, *J. Chem. Phys.* **72**, 6209 (1980).
- ²¹D. G. Truhlar, J. A. Merrick, and J. W. Duff, *J. Am. Chem. Soc.* **98**, 6771 (1976).
- ²²J. C. Gray, D. G. Truhlar, and M. Baer, *J. Phys. Chem.* **83**, 1045 (1979).
- ²³W. Jakubetz, *Chem. Phys.* **88**, 271 (1984).
- ²⁴M. Baer, *J. Chem. Phys.* **60**, 1057 (1974).
- ²⁵J. N. L. Connor, J. C. Whitehead, W. Jakubetz, and A. Lagana, *Nuovo Cimento* **63B**, 116 (1981).
- ²⁶H. Essen, G. D. Billing, and M. Baer, *Chem. Phys.* **17**, 443 (1976).
- ²⁷A. M. G. Ding, L. J. Kirsch, D. S. Perry, J. C. Polanyi, and J. L. Schreiber, *Faraday Discuss. Chem. Soc.* **55**, 252 (1973).
- ²⁸M. D. Pattengill, J. C. Polanyi, and J. L. Schreiber, *J. Chem. Soc. Faraday Trans. 2* **72**, 897 (1976).
- ²⁹R. L. Wilkins, *J. Chem. Phys.* **63**, 2963 (1975).
- ³⁰J. N. L. Connor, A. Lagana, J. C. Whitehead, W. Jakubetz, and W. Manz, *Chem. Phys. Lett.* **62**, 479 (1979).
- ³¹J. N. L. Connor, W. Jakubetz, A. Lagana, W. Manz, and J. C. Whitehead, *J. Chem. Phys.* **65**, 29 (1982).
- ³²B. M. D. D. Jansen op de Haar, G. G. Balint-Kurti, and R. E. Wyatt, *J. Phys. Chem.* **89**, 4007 (1985).
- ³³J. M. Alvarino and A. Lagana, *J. Mol. Struct.* **93**, 271 (1985).
- ³⁴A. Lagana, *J. Chem. Phys.* **86**, 5523 (1987).
- ³⁵A. Lagana, E. Garcia, and J. M. Alvarino, *Nuovo Cimento* **12D**, 1529 (1990).
- ³⁶B. Hildebrandt, H. Vanni, and H. Heydtmann, *Chem. Phys.* **84**, 125 (1984).
- ³⁷J. C. Polanyi, J. L. Schreiber, and J. J. Sloan, *Chem. Phys.* **9**, 403 (1975); J. C. Polanyi, J. J. Sloan, and J. Wanner, *ibid.* **13**, 1 (1976).
- ³⁸The fraction of energy entering a product mode (x) is defined as $f'_{(x)} = \langle E'_x \rangle / E'_{\text{TOT}}$, where $\langle E'_x \rangle$ is the average energy entering the product mode x and E'_{TOT} is the total energy available to the products.
- ³⁹E. J. Kruus and J. J. Sloan, in *Advances in Spectroscopy*, edited by R. J.

H. Clark and R. E. Hester (Wiley, New York, 1989), Vol. 18, Chap. 5.

⁴⁰P. A. Berg and J. J. Sloan, *Rev. Sci. Instrum.* **64**, 2508 (1993).

⁴¹R. E. Continetti, B. A. Balko, and Y. T. Lee, *Chem. Phys. Lett.* **182**, 400 (1991).

⁴²E. Arunan, D. W. Setser, and J. F. Ogilvie, *J. Chem. Phys.* **97**, 1734 (1992).

⁴³L. T. Cowley, D. S. Horne, and J. C. Polanyi, *Chem. Phys. Lett.* **12**, 144 (1972).